Is the fate of clinical candidate Arry-520 already sealed? Predicting resistance in Eg5-inhibitor complexes

Rose-Laure Indorato[1], Sandeep K. Talapatra[2,4], Fangzhu Lin[2], Shozeb Haider[2], Simon P. Mackay[3], Frank Kozielski[2⋆], Dimitrios A. Skoufias[1⋆]

Affiliations:

[1]Université Grenoble Alpes, CNRS, CEA, Institut de Biologie Structurale (IBS), 38000 Grenoble, France

[2]Department of Pharmaceutical and Biological Chemistry, UCL School of Pharmacy, 29-39 Brunswick Square, London, WC1N 1AX, United Kingdom

[3]Strathclyde Institute of Pharmacy and Biomedical Sciences, University of Strathclyde, Glasgow, G4 0NR, United Kingdom

[4]Current Address: Discovery Biology, Discovery Sciences, IMED Biotech Unit, AstraZeneca, Alderley Park, United Kingdom

Conflict of Interest

The authors declare no competing interests.

⋆Correspondence:
dimitrios.skoufias@ibs.fr; tel: +33 (0)4 57 42 86 16
f.kozielski@ucl.ac.uk; tel: +44(0)2077535879

Running Title: Eg5 binding and acquired resistance to Arry-520 inhibitor

Abstract

Arry-520 is an advanced drug candidate from the Eg5 inhibitor class undergoing clinical evaluation in patients with relapsed or refractory multiple myeloma. Here we show by structural analysis that Arry-520 binds stoichiometrically to the motor domain of Eg5 in the conventional allosteric loop L5 pocket in a complex that suggests the same structural mechanism as other Eg5 inhibitors. We have previously shown that acquired resistance through mutations in the allosteric binding site located at loop L5 in the Eg5 structure appears to be independent of the inhibitors' scaffold, which suggests that Arry-520 will ultimately have the same fate. When Arry-520 was assessed in two cell lines selected for the expression of either Eg5(D130A) or Eg5(L214A) STLC-resistant alleles, mutations previously shown to convey resistance to this class of inhibitors, it was inactive in both. Surprisingly, when the cells were challenged with ispinesib, another Eg5 inhibitor, the Eg5(D130A) cells were resistant, but those expressing Eg5(L214A) were strikingly sensitive. Molecular dynamics simulations suggest that subtle differences in ligand binding and flexibility in both compound and protein may alter allosteric transmission from the loop L5 site that do not necessarily result in reduced inhibitory activity in mutated Eg5 structures. Whilst we predict that cells challenged with Arry-520 in the clinical setting are likely to acquire resistance through point mutations in the Eg5 binding site, the data for ispinesib suggests that this resistance mechanism is not scaffold independent as previously thought, and new inhibitors can be designed that retain inhibitory activity in these resistant cells.

Introduction

Over the last two decades, the role of the kinesin motor protein Eg5 (also known as Kinesin Spindle Protein, KSP and coded by the Kif11 gene) in spindle formation and as a target for the development of novel antimitotic agents has been intensively investigated (1). Eg5, like many other kinesins, uses the chemical energy released by its hydrolysis of ATP to generate the force required to move unidirectionally along MTs (2). Eg5 is a plus-end directed motor (2) which, through its antiparallel homotetrameric nature (3), is capable of cross-linking antiparallel overlapping MTs during mitosis and is responsible for centrosome separation and spindle bipolarity (4). Since the discovery of monastrol (5), a small molecule inhibitor of Eg5 capable of inducing mitotic arrest in cells through the formation of monoastral spindles and the subsequent failure of duplicated centrosomes to separate, a large number of Eg5 inhibitors have been developed, with some entering clinical trials (6).

Most Eg5 inhibitors target a specific allosteric site in its motor domain composed of helix α2/loop L5 and helix α3 (7), which is approximately 10 Å away from the ATP binding site. Binding to this pocket induces a rearrangement of loop L5, which allosterically transmits conformational changes in the ATP binding pocket, slowing down ADP release. As a result, Eg5 is trapped in an ‘‘ATP-like’’ conformation and the mechanochemical cycle of the motor is inhibited (8),(9),(10). More recently, another group of Eg5 inhibitors has been found to bind to a different allosteric pocket of the Eg5 motor domain formed by helices α4 and α6 (11),(12),(13),(14).

Although a number of loop L5 binding agents have entered clinical trials, results have been disappointing across various tumor types (15). One possible explanation for the poor clinical efficacy of Eg5 inhibitors in these trials may be the observation that in solid tumours, cells

divide more slowly and not at the high rates observed in mice tumour xenografts thus limiting the number of mitotic cells responding to Eg5 inhibition during chemotherapy at the concentrations administered (16).

Recently however, the Eg5 inhibitor Arry-520 (approved name filanesib; Figure 1a) has proved to be effective in phase I and II clinical trials involving patients with soft tissue cancers, particularly in those with relapsed or refractory multiple myeloma (17),(18), and has since progressed to a phase III clinical trial. Arry-520 has a tolerable safety profile with an improved pharmacokinetic profile compared to other Eg5 inhibitors and encouraging efficacy when administrated as a monotherapy or in combination with proteasome inhibitors in patients heavily pretreated with other chemotherapeutic agents (19). Furthermore, results from clinical trials also indicated a relationship between the expression levels of α-1 acidic glycoprotein (AAG) and the efficacy of Arry-520: low levels of AAG in the serum of patients were correlated with a better chemotherapeutic index compared to higher AAG levels (19).

The success of Arry-520 against haematological malignancies in the clinic has been linked to the lower stability of the Mcl-1 anti-apoptotic protein during mitotic block in these cell types (20). Exposure to Arry-520-induced Eg5 inhibition promotes Mcl-1 degradation during mitotic block, which diminishes the pro-survival signals and allows the apoptotic pathway to be initiated unhindered. Tumour cells less responsive to Eg5 inhibition have survival signals dependent on other members of the anti-apoptotic family such as Bcl-2 or Bcl-XL. These proteins exhibit slower degradation profiles during mitotic block compared to Mcl-1, and may still be capable of inducing their pro-survival signals in response to Eg5 inhibition and mitotic arrest, leading to less efficient cell death in these tumour types (21).

Emergence of resistance to any drug treatment for cancer is often encountered in the clinic and one would expect the same to occur in tumor cells exposed to anti-Eg5 inhibitors. Whilst no clinically relevant Eg5 mutations have been reported to date that are involved in the development of resistance clinically, what has been shown in tumour cells constantly exposed to Eg5 inhibitors is the adaptation and use of alternative pathways to progress to a bipolar spindle. These include overexpression of other members of the kinesin family such as Kif15 (22),(23) or reduced expression of proteins such as dynein that oppose Eg5 activity in centrosome separation (24). Resistance to inhibitors may also arise through point mutations in the Eg5 inhibitor binding pocket (25),(26),(10),(27). Mutations in the helix α2, loop L5 and helix α3 allosteric binding site of Eg5 have been shown to confer resistance in cells to monastrol and a variety of other loop L5 inhibitors (28) including STLC (29), a compound previously identified by our group (30). Notably, we have shown that mutations to specific residues in the inhibitor-binding site (including D130A; D130V; D133A and L214A), can overcome inhibition by blocking the allosteric communication network to the ATP binding site (31). We also demonstrated that these mutations were scaffold independent and can confer resistance across different loop L5 binding inhibitors (28). Whether any of these point mutations can induce resistance to the advanced clinical candidate Arry-520 is not yet known, but the results from our earlier studies suggest that this is possible, which could have implications for its clinical success.

To date, the structure of Arry-520 complexed with Eg5 has not been reported. If it binds to the loop L5 region like other inhibitors, the potential for resistance to develop is increased. The focus of this study was to establish whether Arry-520 was a loop L5 binding allosteric inhibitor by determining the structure of the complex, and given its progression to Phase III clinical trials, whether resistance is likely via point mutations in the allosteric site that have

previously been shown to be scaffold independent. To explore this, we compared the activity of Arry-520 with another important Eg5 inhibitor ispinesib in cell lines expressing the STLC-resistant D130A or L214A alleles of Eg5 in order to evaluate whether resistance could develop to these significantly different scaffolds. Ispinesib itself has previously been through extensive phase I and phase II clinical trials evaluation (32).

Our structural data demonstrates that Arry-520 binds to the same helix α2, loop L5 and helix α3 allosteric site as ispinesib (33), monastrol (7) and STLC (34). Furthermore, our cell-based assays show that cells expressing either the Eg5 D130A or the L214A allele were both resistant to Arry-520. However, whilst resistance to ispinesib was conferred by the D130A mutation as predicted, the L214A expressing cells remained highly sensitive to it. Using molecular dynamics simulations, we identify that a subtle difference in conformational flexibility between Arry-520 and ispinesib is responsible for the difference in inhibitory activity against the L214A mutant. We discuss the significance of these results with respect to differential binding to wild type and mutant states at the molecular level and the implications this has for emerging drug resistance when using drugs that target the allosteric-binding site of Eg5.

Materials and Methods

Cell tissue culture

U2OS cells were obtained from ATCC (ATCC® HTB96™) and were characterized and authenticated by ATCC and not by the authors using a comprehensive database of short tandem repeat DNA profiles. The previously selected STLC resistant clones U2OS-Eg5(D130A) and U2OS-Eg5(L214A) (28) were grown in D-MEM (Gibco BRL; Paisley, UK), supplemented with 10% fetal calf serum (Hyclone) in the absence or presence of 10 μM STLC (Novabiochem, Merck KGaA, Darmstadt, Germany). The cells were not tested for *Mycoplasma*. Before exposure to Arry-520 or ispinesib, cells were washed with STLC-free media three times for 5 min and then replaced with medium containing either 10 nM of Arry-520 (TOCRIS Bioscience) or ispinesib (TOCRIS Bioscience).

Immunofluorescence microscopy

Cells were grown on poly-D-lysine (Sigma-Aldrich, Saint Louis Missouri)-coated 12-mm-diameter glass coverslips and then exposed for 8 h to 10 μM STLC (from 50 mM stocks in DMSO), 10 nM Arry-520 or 10 nM ispinesib (from 10 μM stocks in DMSO) at 37°C. Cells were then fixed by incubation in 2% paraformaldehyde (20 min at 37 °C) and permeabilized with 0.2% Triton X-100 in PBS for 3 min before being incubated with primary and stained with secondary antibodies. MTs were detected by a mouse monoclonal anti-β-tubulin antibody (SIGMA) used at 400-fold dilution. The Alexa fluo-488 goat anti-mouse secondary antibodies (Invitrogen) were used at 400-fold dilution, respectively. DNA was detected with 4',6-diamidino-2-phenylindole dihydrochloride (DAPI) with the VECTASHIELD (Vector Laboratories Inc, Burlingame, CA) mounting medium.

Images were collected with an inverted Olympus IX81 epifluorescence motorized microscope equipped with a motorized piezo stage (Ludl Electronic Products, USA) and a sCMOS (Hamamtsu Orca Flash4) camera driven by VOLOCITY software (Improvision Ltd, UK) with a binning of 1, using a PlanApo 60x NA1.42 objective (Olympus). Images were processed in Adobe Photoshop CS5 (Adobe) and assembled in Adobe Illustrator (Adobe). Mitotic cells were scored based on their phenotypes in triplicates, as either bipolar or monoastral.

Flow Cytometric Analysis

Cells were first fixed and labeled with propidium iodide as described previously. Data were collected with a MACSQuand instrument (Miltenyi Biotec, Germany). For each sample 10,000 events were collected and aggregated cells were gated out.

Crystal violet colony staining of U2OS STLC resistant clones

Cells (2k cells/ plate) were plated in 6-well plates and the day after seeding, cells were treated with the inhibitors. The media was changed every four days and on day 10, when colonies started appearing visible cells were washed twice with ice cold PBS and fixed with 100% ice cold methanol for 10 min. Then the cells were stained with 0.5% crystal violet in 25% ice cold methanol for additional 10 min. Following excessive washes with double distilled water the plates were dried at room temperature and then images were taken using a scanner. For quantification of crystal violet staining, cells were plated at a density of 17,000 cells per well on a 24-well plate and subjected to the indicated concentrations of inhibitors. After 4 days, cells were washed with PBS, fixed with 4% paraformaldehyde for 20 min, stained with 0.5% crystal violet (C3386, Sigma-Aldrich) for 30 min, rinsed with deionized water, and air dried. Crystal violet solution was then solubilized using 10% acetic acid for 20 min, diluted 1:4 with deionized water and the absorbance (595 nm) was read using an Eppendorf Biophotometer.

Live cell imaging

Cells were grown in 2-well Labtek chambers and just before recording, the medium was changed to DMEM/F-12, HEPES, without phenol red, supplemented with 10% fetal bovine serum and either 10 μM STLC, 10 nM Arry-520 or 10 nM Ispinesib. Cells were recorded with an inverted Olympus IX81 microscope with a DIC 20x objective (1 NA) binning of 1 equipped with an environmental control chamber using a sCMOS (Hamamtsu Orca Flash4) camera driven by VOLOCITY software. Images were acquired at 3 min intervals. For analysis, at least 100 cells were followed for 16 h and for each condition the time of each cell spent in mitosis was recorded. The duration of mitosis for each cell was measured from the first time point that an interphase cell started to contract before becoming circular until the end of cytokinesis when the two daughter cells started to spread. Cells undergoing normal cytokinesis were scored as normal mitosis whereas cells that did not undergo cytokinesis and remained circular were scored as blocked in mitosis. Cells undergoing cytokinesis of tripolar spindles, slippage or death were scored as aberrant mitotic exits.

Expression and purification of human Eg5

Cloning, expression and purification of the motor domain of Eg5 (residues 1–368) was performed as described previously (Kaan et al., 2010)(34).

Isothermal titration calorimetry (ITC) experiments

ITC experiments were performed as previously described in Talapatra et al, 2013 (31) with minor modifications. Eg5 was used at a concentration of 12.5 μM for the ITC experiments. Inhibitors were diluted to an appropriate concentration in ITC buffer (50 mM HEPES pH 6.8, 200 mM NaCl, 0.5 mM ADP and 2 mM $MgCl_2$) so that the final solution contained no more

than 1% DMSO. To maintain a similar buffer composition for titrations, 1% DMSO was added to the protein solution. Arry-520 was used at a concentration of 100 μM. There were no detectable solubility issues at these concentrations. ITC experiments were performed with a MicroCal PEAQ-ITC (Malvern Instruments, UK) instrument. Titrations were carried out at 25°C with a stirring speed of around 750 rpm. In total, 30 injections were performed for one protein inhibitor experiment with the first injection of 0.3 μL followed by 29 injections of 1.3 μL and a gap of 120 s between each injection. Data analyses were performed after subtraction of the heats of dilution obtained from titration of Arry-520 into ITC buffer. The thermodynamic parameters N (stoichiometry), K_d (dissociation constant/binding affinity), ΔS (entropy change) and ΔH (enthalpy change) were obtained by using the single-site-binding model of the PEAQ-ITC analysis software (Malvern Instruments, UK). For each experiment, at least two titrations were performed. Titration data were analysed independently, and the means of obtained values reported.

Crystallisation, structure determination and refinement of Eg5-Arry-520 complexes

Eg5 at 10 mg/ml was incubated with 2 mM of Arry-520 for 2 h at 4°C before crystallisation trails. Initial crystals of the complex in space-group $P2_12_12_1$ were obtained after one week at 4 °C on mixing 1 μl of the Eg5 complex with 1 μl of either condition 1 (0.1 M MES pH 5.5, 25.5% PEG 3350 and 0.25 M $(NH_4)_2SO_4$) or condition 2 (0.1 M HEPES pH 6.5, 0.2 M K_2HPO_4 and 33% PEG 3350) buffer by vapor diffusion in sitting drops. Crystals in space-group $P3_2$ appeared in 0.04 M KH_2PO_4 and 12.5% PEG 8000 after 3 days. For data collection, diffraction quality single crystals were cryo-protected using 1.2x the concentration of the well solution and 15% (v/v) glycerol. The crystals were then flash frozen in liquid nitrogen for subsequent measurements using synchrotron radiation.

Diffraction data were collected at beamline I03 and 104-1 at Diamond Light Source. Data were processed and scaled using either iMosflm or XDS (35) and truncated using SCALA from the CCP4 suite of programs (36). The structures of the Eg5-Arry-520 complexes were solved by molecular replacement (PHASER MR in CCP4 suite) using the native Eg5-monastrol structure (PDB code 1X88, (37) as a search model. All structures were initially refined with REFMAC5 (38). Electron density and difference density maps, all σA-weighted, were inspected, and the models were improved using Coot (39). The refinement of the structure was performed using PHENIX. The calculation of R_{free} used 5% of data. Crystallographic and refinement statistics are given in Supplementary Data Table S1.

In both structures, several regions are flexible and not visible in the electron density. In space group $P2_12_12_1$ with two molecules in the AU, molecule A covers residues Lys17 to Asn29, His38 to Thr249, Leu255 to Asn271 and Asn287 to Val365. In molecule B, the following residues are visible: Lys17 to Ala31, His38 to Gly56, Ser61 to Asn271 and Asn287 to Glu364. Space group $P3_2$ contains three molecules in the AU and comprises the following residues. Molecule A: Ala16 to Glu247, Glu254 to Asn271 and Asn287 to Glu364. Molecule B: Lys17 to Lys246, Leu255 to Asn271 and Asn287 to Glu364. Molecule C: Lys17 to Asn271, Asn287 to Leu302 and Val309 to Pro363.

Molecular Dynamics Simulations

The crystal structure of Eg5 in complex with ispinesib (PDB ID 4A5Y) and SB743921 (PDB ID 4AS7) were downloaded from the protein data bank (www.rscb.org). The 4AS7 structure, which has complete loops for residues 30-37 and 272-286, was used as a template to model the missing loops in the Eg5-Arry-520 complex described in this study. Additionally, the 4AS7 structure is an A133D mutant with a cadmium ion. The side chain of Asp133 in loop L5

was replaced with Ala at position 133 without any change in the backbone conformation using the ICM-Pro software (www.molsoft.com) and cadmium was mutated to magnesium. The structural analog SB743921 in 4AS7 was replaced with ispinesib by superimposition of the two structures and retaining the coordinates of ispinesib. The Eg5(L214A) mutant in α3 helix was generated by replacing the side chain of Leu with Ala in the modeled Eg5 structure. The backbone root mean square deviation calculated over 347 residues between the Eg5(L214A)-ispinesib and the Eg5(L214A)-Arry520 complex is 0.36 Å and that between Eg5(D130A)-ispinesib and the Eg5(D130A)-Arry520 complex is 0.12 Å. Parameters for the ligands were generated using antechamber software (40) after geometry optimization at the B3LYP/6-31G(d) level and RESP charge fitting (41) using electrostatic potential obtained at the HF/6-31G(d) level. The parameters of ADP were adapted from Meagher *et al*(42). The complexes were set up using xleap employing the ff14sb forcefield (43) for the protein and GAFF2 for the ligands. The complexes were solvated using TIP3P water (44) and the edge of the box was set to at least 10 Å from the closest solute atom. The system was neutralized with K+ and Cl- ions. The protocol was identical for all systems. Each system was minimized and relaxed under NPT conditions for 5 ns at 1 atm. The temperature was ramped up to 298K using a timestep of 4 fs, rigid bonds, a cut-off of 9 Å and a particle mesh Ewald summations switched on for long-range electrostatics. Only the solvent and ions were allowed to move during the equilibration. The heavy atoms of the protein and ligands atoms were constrained by a spring constant set at 1 kcal/mol/$Å^2$. The production simulations were run using ACEMD (45) molecular dynamics engine in the NVT ensemble using a Langevin thermostat with a damping of 0.1 ps^{-1} and hydrogen mass repartitioning scheme to achieve time steps of 4 fs (46). The final production step was run without any constraints for 555 ns. The analysis was carried out using the final 255 ns of simulation time. Visualization of the simulation was done using ICM-pro Molsoft and VMD package (47).

Results

Determination of the binding affinity of Arry-520 for Eg5 by isothermal titration calorimetry (ITC)

The IC_{50} of Arry-520 against Eg5 has previously been reported as low nanomolar using a kinetic ATPase activity assay (48). To measure the binding affinity of Arry-520 for Eg5, we employed a biophysical assay using our well-established ITC protocol for high affinity inhibitors (12), which showed that Arry-520 is a tight-binding inhibitor with a K_d value of ~ 460 pM (Figure 1b) in the absence of MTs. Thermodynamic parameter extraction from the ITC experiments indicated a profile similar to our previous analysis of the ispinesib analogue SB743921 with wild-type Eg5. Like SB743921, binding between Arry-520 and Eg5 is primarily driven by an enthalpic contribution, although there is a small positive entropic contribution rather than a penalty with this ligand. Data analysis indicated that the binding data fit well to a single binding site model with a stoichiometry close to unity, signifying a 1:1 complex with the Eg5 motor domain similar to most other loop L5 binding agents and suggesting that Eg5-Arry-520 co-crystallization was likely to succeed.

Overall description of two Eg5-Arry-520 complexes in two distinct space groups

Two structures of the Eg5-Arry-520 complex in two different space groups were solved at 2.8 Å and 2.75 Å resolution and were refined to R_{free} values of 27.1% and 25.2%, respectively. Data processing and refinement statistics are shown in Supplementary Data Table S1.

Crystals in space group $P2_12_12_1$ contain two molecules of Eg5 in the asymmetric unit (AU), each bound with Arry-520, whereas those obtained in space group $P3_2$ contain three complexes in the AU. All five motor domain structures fit to the canonical kinesin motor domain fold with an eight-stranded β-sheet sandwiched between three major α-helices on each side (Figure 1c). Each motor domain has one molecule of Mg^{2+}ADP bound in the

nucleotide-binding pocket. In all five motor domain structures, Arry-520 occupies the conventional allosteric inhibitor-binding pocket formed by helix α2, loop L5 and helix α3 (Figure 1d). In the Eg5-Arry-520 complexes, the loop L5 region is ordered and visible (Figure 1d) unlike in the unbound structure of Eg5, where this region is mostly disordered and absent (49).

Eg5-Arry-520 complexes in the intermediate and final inhibitor bound state

Comparison of the five Eg5-Arry-520 complexes from two distinct space groups with the native unbound Eg5 structure (PDB entry 1II6; (49)) reveals major structural changes in the switch II cluster (helix α4/loop loop L12 and helix α5) and the so-called neck-linker region (Supplementary Figure S1). The binding of Arry-520 to the loop L5 region induces conformational changes in and around the inhibitor-binding pocket (switch I), which are transmitted to the switch II cluster and the neck-linker region following helix α6. Both intermediate and final inhibitor bound states are evident in our structures: in space group $P3_2$, one of the three molecules in the AU (molecule C) is in the intermediate bound state, where the switch II cluster is in the obstructive conformation forcing the neck linker region to be perpendicular to the motor domain (Supplementary Figure S1b). In contrast, the other complexes in space groups $P2_12_12_1$ and $P3_2$ are in the "final" inhibitor bound state. In this conformation, the switch II cluster is in the permissive conformation, which enables the neck-linker to dock to the motor domain (Supplementary Figure S1b). These conformational states have previously been observed in Eg5 complexes with STLC (34) and ispinesib (33),(50) and strongly suggest that Arry-520, by binding to the L5 allosteric inhibitor pocket, invokes a very similar structural mechanism to other Eg5 inhibitors.

Detailed molecular interactions between Eg5 and Arry-520

In all five Eg5-Arry-520 complexes the inhibitor is buried in the allosteric inhibitor-binding pocket. Overall, the binding conformations and interactions of Arry-520 with residues in the inhibitor-binding pocket in all complexes are very similar (Figure 1e & Supplementary Figure S1c). The 2-phenyl group is oriented towards the protein interior and engages in hydrophobic interactions with a range of side chains including Trp127, Pro137 (both T-face edge-to-face stacking aromatic interactions), a π-cation interaction with the guanidine group of Arg119 and a hydrophobic interaction with the propyl region of its side chain and with the methyl group of Ala133. Several main chain carbonyl oxygen atoms are also in close vicinity to the 2-phenyl group. The 2,5-difluorophenyl substituent is also buried in the inhibitor-binding pocket and is sandwiched between the side chains of the conserved Glu116-Arg221-Glu162 ion pair (forming a π-cation interaction with the guanidine group of Arg 221) and Leu214, and is surrounded by a variety of other hydrophobic side chains (Ile136, Phe239 and Leu160). Although the 1,3,4-thiadiazole ring does not display short range interactions with residues of the binding pocket, its geometry facilitates the optimal positioning of its four substituents with different regions of the binding site. We observe subtle conformational flexibilities within the solvent-orientated methoxy group of the *N*-methoxy-*N*-methyl substituent and the primary propylamine moiety. The position/conformation of the primary amine oscillates slightly and forms hydrogen bond interactions with the side chain of Glu116 (2.7 Å - 4.1 Å) and the main chain carbonyl oxygen of Gly117 (2.9 Å - 3.7 Å) simultaneously, whilst the side chain of Glu118 appears to be too far away (5.7 Å – 6.4 Å) to form any effective hydrogen bond interactions. We also observe variation in the conformation of the *N*-methoxy substituent, which forms a hydrogen bond interaction between its oxygen and the side chain hydroxyl of Tyr211 (2.7 Å - 3.1 Å). The methyl groups of this *N*-methoxy-*N*-methyl substituent form hydrophobic interactions with the side chains of Ala218 and the hydrophobic ethyl region of the Glu215 side chain.

The structure of the Eg5-Arry-520 complex demonstrates that Arry-520 binds to the same allosteric pocket as other Eg5 loop L5 binding inhibitors and interacts with a number of common residues within this site (33). This therefore raised the question as to whether known mutations in the allosteric pocket responsible for conferring resistance to inhibitors such as STLC (30) and monastrol (5) could also induce cellular resistance to Arry-520. To answer this question, we assessed Arry-520 against two clones of U2OS tumor cells selected for growth in the presence of STLC through the expression of mutant alleles of Eg5 for each of the D130A or L214A residues (28), and compared the phenotypes with the clinically evaluated inhibitor ispinesib (SB-715992; multiple phase I and II trials) (51).

Cell cycle progression of U2OS cells expressi*ng either Eg5(D130A) or Eg5(L214A) STLC resistant clones in the presence of Arry-520 or ispinesib*

The impact on cell cycle progression after 24 h exposure to the three Eg5 inhibitors was first studied by flow cytometric analysis (Figure 2a). Naïve U2OS cells exposed to either STLC, Arry-520 or ispinesib were blocked at the G2/M stage with 4N DNA content. In contrast to the naïve cells, Eg5(D130A) and Eg5(L214A) expressing cells were cycling normally both in the absence and presence of either STLC or Arry-520. However, in the presence of ispinesib, only the Eg5(D130A) expressing cells showed normal cell cycle profiles. Eg5(L214A) expressing cells, although fully resistant to either STLC or Arry-520, were still highly sensitive to ispinesib, as they accumulated in G2/M.

Spindle formation in naive U2OS cells and in STLC resistant clones of U2OS expressing either Eg5(D130A) or Eg5(L214A) in the presence of Arry-520 or ispinesib

The cell cycle profile of both STLC-resistant cell lines indicated that the cells were able to divide normally in the presence of Arry-520. To confirm the presence of normal bipolar spindles in these cells exposed to Arry-520 and in order to identify the phenotype of the Eg5(L214A) expressing cells blocked in G2/M in the presence of ispinesib, we carried out indirect immunofluorescence microscopy. Naïve U2OS cells and cells from the Eg5(D130A) and Eg5(L214A) U2OS clones were exposed to either STLC, Arry-520 or ispinesib. As expected, all three inhibitors induced monoastral spindles in the naïve cells due to the inhibition of Eg5 activity: MTs were nucleated from the duplicated but not-separated centrosomes extending into the cytoplasm in a monoaster configuration while chromosomes were distributed along the MT in a centripetal fashion (Figure 2b). The vast majority of the spindles (close to 100%) were monoastral (Figure 2c). In contrast to the naïve U2OS cells, cells expressing the Eg5(D130A) mutant allele were capable of forming normal bipolar spindles in the presence of all three inhibitors and proceeded normally to anaphase. At concentrations at which all three inhibitors produce 100% inhibition in the naïve cells, only 20% of the spindles were monoastral in the presence of STLC and Arry-520 and 47% in the presence of ispinesib in the Eg5(D130A) expressing cells. A more striking difference was observed in cells expressing the Eg5(L214A) mutant allele: only 19% and 11% were monoastral in the presence of STLC or Arry-520, respectively, indicating no sensitivity to these inhibitors, whereas the vast majority of the spindles in this mutant were monoastral (99%) when exposed to ispinesib, indicative of high sensitivity (Figure 2b).

Duration of mitosis in naïve U2OS and in Eg5(D130A) or Eg5(L214A) expressing cells in the presence of allosteric Eg5 inhibitors

The ability of the two STLC-resistant U2OS clones to undergo regular cell division following normal bipolar spindles formation and enter into anaphase in the presence of the three

inhibitors was further examined by time-lapse imaging (Supporting Videos SV1-6). The time spent in mitosis for more than 100 cells from all three cell lines in the presence of the inhibitors was measured and compared to that of the untreated cells (Figure 3). Cells undergoing standard mitosis resulting in normal cytokinesis were scored as normal M. Cells that underwent tripolar anaphase resulting in three daughter cells or underwent aberrant mitotic exit without cytokinesis or entered death, were scored as aberrant M exit. Cells that entered mitosis as judged by their morphological changes from the spread interphase configuration to a round shape (and remaining so) throughout the period of observation were scored as arrested in M (Table 1).

The vast majority (94.8%) of the untreated naïve U2OS cells completed mitosis normally. 90.1% of the mitotic cells completed mitosis in less than 1 h, with 97.2% completion achieved in less than 2 h (Tables 1 and 2). In contrast, only 1.3% of the naïve U2OS cells completed mitosis successfully following treatment with Arry-520. As expected from our previous observations (28), the majority of the mitotic cells expressing either Eg5(D130A) or Eg5(L214A) completed mitosis in the presence of STLC normally (89.8% and 94.5%, respectively). As with the naïve cells, the majority of these cells completed mitosis within 1 h and almost all of them within 2 h (Table 2). When treated with Arry-520, both the Eg5(D130A) and Eg5(L214A) expressing cells were capable of completing normal mitosis, reaching 51.4% and 91.8%, respectively, although the former cell line experienced longer mitotic delays; 51.8% of the mitotic cells completed mitosis within 1 h and 67.7% in less than 2 h (Figure 3). The Eg5(L214A) expressing cells passed through mitosis within similar duration as the naïve untreated U2OS. In the presence of ispinesib, the Eg5(D130A) expressing cells divided normally without experiencing any notable mitotic delays, whereas

the Eg5(L214A) cells were blocked in mitosis (84.6%) and displayed monoastral spindles (Figure 2b & c).

Colony formation of U2OS cells expressing either Eg5(D130A) or Eg5(L214A) STLC resistant clones in the continuous presence of Arry-520 or ispinesib.

The differential sensitivity of the cells to the antiproliferative effect of the inhibitors was investigated by assessing colony formation after prolonged exposure (10 days) (Figure 3b). Colonies were readily visible in all three untreated cell lines; naïve cells treated with STLC, Arry-520 or ispinesib were incapable of proliferation and did not form colonies. Eg5(D130A) expressing cells showed resistance to the antiproliferative effects by readily forming colonies in the presence of the three inhibitors. In contrast, Eg5(L214A) expressing cells were capable of colony formation in the presence of both STLC and Arry-520, but not in the presence of ispinesib, indicating their susceptibility to the antiproliferative effects of the latter only. Quantification of crystal violet staining of treated cells confirmed the marked lack of viability of Eg5(L214A) expressing cells exposed to ispinesib (Figure 3c and d) compared to similarly treated Eg5(D130A) expressing cells.

Taken together, our cell-based assays indicate that mutations in the loop 5 allosteric binding pocket that confer resistance to inhibitors such as STLC and monastrol also affect Arry-520. In the case of ispinesib, although resistance occurred in the Eg5(D130A) expressing cells, the Eg5(L214A) cell line was highly sensitive to its antimitotic effects, suggesting that the L214A mutation does not adversely impact the inhibitory mechanism that this particular scaffold has on Eg5.

Molecular dynamics simulations of Eg5 and Eg5(L214A) in complex with Arry-520 and ispinesib.

In order to explore the subtle differences between the binding of inhibitors to the allosteric site in the Eg5 wild type and mutant complexes, we carried out conformational sampling via molecular dynamics simulations. Eg5 has previously been co-crystallized with ispinesib (PDB ID 4A5Y) and a related analogue SB743921 (PDB ID 4AS7), which both occupy the allosteric site in an orientation similar to the one described for Arry-520 in this study (Supplementary Figure S2). The quinazolin-4-one ring of ispinesib occupies an internal hydrophobic pocket that is sandwiched between the Glu116-Arg221 ion-pair (Supplementary Figure S2d) and the aliphatic side chain of Leu214 in the wild type complex. The rest of the scaffold makes non-bonded interactions around the predominantly hydrophobic binding site (Supplementary Figure S2b). The difluorophenyl ring of Arry-520 is sandwiched in a similar way to the quinazolinone ring of ispinesib in the wild type structure (Supplementary Figure S2a and c). From these structures, the mutant complexes were generated by replacing the Leu or Asp side chains with Ala. The ΔΔG of the Leu to Ala change was 0.22 kcal/mol and results in an enlargement of the binding pocket from 297 $Å^3$ to 306 $Å^3$. For the Asp to Ala change, the ΔΔG of was 0.68 kcal/mol and changes the binding pocket volume from 395 $Å^3$ to 404 $Å^3$. The complexes were then subjected to molecular dynamics simulations to extract changes in the flexibility of Arry-520 and ispinesib due to structural perturbations induced in the allosteric binding site as a consequence of either the L214A or D130A mutation (Figure 4a-c' and Supporting videos SV7-SV12). Four simulations were run for 555 ns each and all analyses carried out on the equilibrated trajectory, which included the final 250 ns of simulation time. The difluorophenyl ring of Arry-520 is sandwiched in a similar way to the quinazolinone ring of ispinesib in the wild type structure. The hydrogen bond interactions formed between the primary amine of Glu117 and the *N*-methoxy groups and the binding site

are stable and maintained throughout the course of the simulation (Supplementary Figure S3). The dihedral angle between the 2,5-difluorophenyl and the 1,3,4-thiadiazole ring in Arry-520 was monitored in all complexes, along with the dihedral angle between the quinazolin-4-one ring and the isopropyl group in ispinesib (Figure 4d & e). In the Eg5(L214A)-mutant complex, ispinesib displays similar interactions and dynamics to that observed in the wild type, which could explain why both are sensitive to inhibition by this molecule. There is little conformational flexibility in the ligand, as exemplified by the rotation of the isopropyl group with respect to the quinazolinone ring oscillating tightly around 70^{o} (Figure 4f). The behavior of Arry-520 in the wild type and L214A complexes is different. In the former, Arry-520 is tightly anchored in the allosteric binding site by hydrogen bonding interactions and the difluorophenyl group is tightly sandwiched between conserved Glu116-Arg221-Glu162 and Leu214 side chains. There is little conformational flexibility displayed by the inhibitor throughout the simulation, suggesting a tight-binding mode. The small entropic contribution ($T\Delta S$ = 2.87 kcal/mol) to the binding free energy (ΔG -12.43 kcal/mol) as determined by ITC supports the low conformational flexibility seen in this simulation. In the Eg5(L214A)-mutant, the primary amine hydrogen bonds with the Glu116 side chain and the Gly117 backbone carbonyl oxygen, similar to that in the wild type (Supplementary Figure S3). However, at ~460 ns, the side chain of Tyr211 rotates away from the site resulting in the loss of the hydrogen bond between the *N*-methoxy oxygen and the hydroxyl group of Tyr211 and greater movement between the two moieties (Supplementary Figure S3d). Arry-520 remains tethered in the allosteric binding site via the hydrogen bond interactions made through the primary amine (Supplementary Figure S3). However, the larger volume of the binding pocket generated as a result of the L214A mutation and the rotation of Tyr211 loosens Arry-520 packing in the internal hydrophobic pocket. This results in enhanced wobbling of the diflurophenyl substituent (Figure 4f upper panel). The difference in flexibility between the

tight-binding in the wild type, and the more flexible conformation in the Eg5(L214A) complex could be responsible for the induction of resistance to Arry-520 in this mutant, in stark contrast to ispinesib.

Analysis of the D130A complex trajectories with ispinesib revealed that the bond angle between the quinazolinone ring and the isopropyl group is stabilized at a different angle (~130^{o}) than observed in wild type Eg5 or Eg5(L214A) (Figures 4b', 5f lower panel), which is due to the conformation adopted by loop 116-135 in the D130A mutant. An ion-pair interaction is formed between Arg119 and Glu125, which is very stable when ispinesib is present. The Arg119 side chain is also positioned perfectly to form a hydrogen-bond interaction simultaneously with the exocyclic amide oxygen of ispinesib, thus restricting rotation around the quinazolinone-isopropyl bond to a different angle than observed in the other ispinesib complexes sensitive to inhibition (Figure 4a'-c', 4f lower panel). We also observed an increase in the flexibility of loop L5 (residues 116 to 135) compared to wild type Eg5 and L214A complexes despite the Arg119-Glu125 tether (Supplementary Figure S3e). This suggests that enhanced flexibility in this region coupled with a different conformation of ligand binding could be responsible for the resistance to ispinesib observed with the D130A mutant.

In this region, the behavior of Arry-520 is similar in all three complexes, suggesting that these specific local interactions are not responsible for wild type sensitivity or mutation-induced resistances to this scaffold. Arg119 does not form any direct stable interactions with Arry-520 and no Arg119-Glu125 ion-pair interactions within the protein are evident.

Discussion

The first two crystal structures of the Eg5-Arry-520 complex convincingly show that Arry-520 is buried in the same conventional inhibitor-binding pocket (α2 / loop L5 / helix α3) as observed for allosteric inhibitors such as ispinesib, STLC and others. Overall, the tight binding of Arry-520 is achieved through a number of strong and weak hydrogen bond interactions as well as hydrophobic interactions with the side chains of amino acids lining the inhibitor-binding pocket. We compared the structure of the Eg5-Arry-520 complex with that of the Eg5-ispinesib complex (PDB ID: 4AP0), (33) (Figure 1f). Superimposition of the two complexes showed that the quinazolinone of ispinesib occupied a similar position to the difluorophenyl ring of Arry-520, with similar interactions such as the chlorine mimicking one of the polar fluorine interactions with Tyr211. An interesting difference between each ligand involves the *p*-toluyl and benzyl groups of ispinesib and the benzyl moiety of Arry-520. In ispinesib, these two aromatic substituents stack with each other, which stabilizes a further stacking interaction with the backbone of Glu118, Arg119 and the side chains of Arg119, Trp127 and Asp130. This backbone stacking interaction is much weaker in the Eg5-Arry-520 complex. A second difference involves the hydrophobic interaction with Leu214. With Arry-520, there is a direct hydrophobic stacking interaction between the difluorophenyl group and the isobutyl side chain of the residue, whereas in the ispinesib complex, the side chain has shifted by 2 Å to accommodate the benzyl and *p*-toluyl groups thereby weakening or losing this interaction altogether. Arry-520 and ispinesib form hydrogen bond interactions between the primary amine and the main chain oxygen of Gly117 and the side chain of Glu116. The oxygen of the methoxy group in Arry-520 may form a weak hydrogen bond interaction with the hydroxyl group of Tyr211 (3.63 Å). Furthermore, one fluorine in the phenyl ring interacts with the main chain NH of Gly217 (3.03 Å) and also weakly with the side chain of Arg221 (3.69 Å). The crystal structure of Eg5 complexed with a 1,3,4-thiadiazole core scaffold has

recently been published (Supplementary Figure S1e) (52). K858 represents a smaller, pre-optimised version of Arry-520 that lacks the key substituents necessary for potent inhibition.

The α2 / loop L5 / helix α3 pocket has been the focus of a number of mutagenesis studies in order to understand not only the mode of interaction of Eg5 with its various inhibitors but also how the ligands exert their allosteric inhibition (26),(10). We have previously shown that mutations in this binding pocket can confer resistance in cells to inhibitors that are known to bind to this pocket, such as monastrol and STLC (29). Notably, we have previously used the expression of the two point mutations D130A and L214A in the Eg5 binding pocket to discriminate loop L5 binding inhibitors from those capable of interacting with other binding sites such as the ATP competitive inhibitors (28). We have shown here that these two STLC resistant cell lines, one harboring and expressing D130A and the other L214A in Eg5, are also resistant to Arry-520 treatment, since the majority of the cells from both cell lines were able to form normal bipolar spindles (Figure 2). Live cell imaging showed that STLC-resistant cell lines treated with Arry-520 did not experience delays in passing through mitosis and divided normally (Figure 3). Flow cytometric analysis showed normal cell cycle profiles for STLC-resistant cells in common with control naïve untreated cells (Figure 2). Finally, exposure to Arry-520 did not inhibit the ability of both STLC-resistant cell lines to form colonies after long exposure. Based on these results, we can conclude that both D130A and L214A mutations in the Eg5 allosteric binding site can confer similar resistance to Arry-520, as they do with STLC. Moreover, they also suggest that the primary, if not the only mitotic target of Arry-520, is indeed Eg5.

An unexpected outcome emerged when comparing the inhibitory activities of the two clinically advanced inhibitors Arry-520 to ispinesib in STLC-resistant cell lines. Both Arry-

520 and ispinesib were ineffective in the Eg5(D130A) expressing STLC-resistant cells, which was to be expected since the D130V allele of Eg5 was previously identified as conferring resistance to ispinesib and its closely related analogue SB743921 (31). However, a significantly different sensitivity to the two inhibitors was seen in the Eg5(L214A) cell line. Although Arry-520 was ineffective in Eg5(L214A) expressing cells in common with STLC and other loop L5 binding inhibitors, ispinesib was still fully capable of inhibiting growth. Monoastral spindle development was evident, cells were blocked in mitosis without proceeding to anaphase (Figure 2) and failed to form colonies after prolonged exposure to ispinesib (Figure 4).

This differential resistance of the Eg5(L214A) expressing cells to Arry-520 and ispinesib appears to challenge our previous proposition of using these two resistant cell lines as tools in phenotype based screening to determine if other novel Eg5 inhibitors bind to the conventional allosteric site of Eg5 without any previous structural information (28). From a structural perspective based on a crystallographic snapshot, this is difficult to rationalize. Leu214 is involved in a network of hydrophobic interactions with the side chains of Ile136, Pro137, Val210 and Phe239 within the allosteric inhibitor-binding cavity and both ispinesib and Arry-520 bind in a similar orientation within this site. The diflurophenyl and the quinazolinone rings are tightly sandwiched between the conserved ion-pair interactions of Glu116-Arg221-Glu162 and the hydrophobic stacking interactions of Leu214, despite its side chain having shifted by 2 Å to accommodate the benzyl and *p*-toluyl groups of ispinesib.

Analysis of the simulated dynamic trajectories of wild type and mutant complexes rather than relying on static structures offers possible explanations for these differences in sensitivity. In ispinesib, the quinazolinone ring has two substituents (isopropyl and benzyl), each connected

to it by a rotatable bond. During the simulations, the rotation around these bonds is restricted in wild type Eg5 by the tight packing of the isopropyl group against the backbone of Leu214 in helix-α3 and the benzyl ring to the side chain of Leu214 (Figure 4). This places ispinesib in a highly constrained and favorable hydrophobic chemical environment, inferring a tight-binding complex that results in effective inhibition. In the Eg5(L214A)-ispinesib mutant complex, despite the removal of the Leu side chain, the increase in volume is not enough to allow greater overall substituent flexibility in the ligand (Figure 4), as exemplified by the restriction of the rotational angle around the isopropyl-quinazolinone bond to the same degree and magnitude as the wild type (Figure 4). Overall, this resulted in a very similar dynamic and interaction profile around the allosteric binding site for both complexes, suggesting tight ligand binding and effective inhibition, which corresponds with the phenotypic outputs from the cell-based experiments conducted with ispinesib. Molecular dynamics simulations of the Eg5(D130A) bound to ispinesib revealed that the bond angle between the quinazolinone ring and the isopropyl group is stabilized at a different angle (Figure 4f), which is due to the conformation adopted by loop L5 and the consequent hydrogen bond interaction between Arg119 and ispinesib. The additional increase in the flexibility of loop L5 compared to the wild type and L214A complexes allows greater conformational freedom within the ligand (Figure 4) thus reducing its tight-binding nature and compromising its ability to inhibit the mutated protein. We have previously shown that the reduced inhibition by the ispinesib analogue SB743921 in the D130V mutant (31) is also due to increased flexibility in this region: the loss of the side chain interaction between Asp130 and the side chains of Ser120 and Arg119 and the main-chain amino groups of Ser120 and Leu132 reduce the structural stability of loop L5. A D130A mutation would compromise this same interaction network, which was reproduced by the higher flexibility of loop L5 in the D130A-ispinesib trajectory reported here.

In the simulated wild-type Eg5-Arry520 complex, hydrogen bonding interactions between the primary propylamino group and Glu116/Gly117 at one end of the ligand and the *N*-methoxy oxygen with the hydroxyl side chain of Tyr211 at the other locks Arry-520 in the allosteric binding site to produce a trajectory with restricted conformational flexibility (Figure 4). Unlike ispinesib, in the Eg5(L214A)-Arry520 mutant, the extra volume in the inhibitor binding pocket generated in the L214A mutation allows greater ligand flexibility, displayed by increased wobbling of the difluorophenyl group around the bond connecting it to the thiadiazole ring (Figures 4f). This appears to be linked with the increased distance between the *N*-methoxy oxygen and Tyr211 induced by the rotation of the amino acid side chain to weaken the hydrogen bond. The enhanced flexibility observed for Arry-520 would compromise its effectiveness as a tight-binding inhibitor, leading to resistance in cells containing this mutation. Comparison of the RMS fluctuation of the wild type and L214A loop 5 regions of the binding site also show greater plasticity in the latter (Supplementary Figure 3e), which is known to compromise allosteric transmission by inhibitors to the ATP binding site in resistant mutants (31). Notably, this region is less flexible in the L214A-ispinesib complex, where inhibition is observed.

To date, targeting Eg5 in cancer with small molecule inhibitors has had mixed outcomes clinically: despite a number of loop L5 binding agents entering clinical trials, results have been poor in solid tumors, whereas haematological cancers look to be more responsive (6). The reduced clinical efficacy of these inhibitors in solid tumors may be due to the low tumour cell proliferation rates and reduced drug penetration associated with these cancer types (16). The adverse reaction of neutropenia in clinical trials, a known consequence of Eg5 target engagement in normal cell proliferation (19), suggests that the efficacies and pharmacokinetic

profiles of the drugs under clinical investigation are not compatible with their narrow therapeutic indices in solid tumour scenarios. The better pharmacokinetic profile of Arry-520 and the associated reduced dosing frequency compared to other Eg5 inhibitors (53), combined with the high proliferation rate of relapsed multiple myeloma cells (14% to 83 %) (54) may be the reason for the better therapeutic index of Arry-520. Its totally different chemical scaffold may also have fewer off-target adverse effects than other Eg5 inhibitors, which may also contribute to a wider therapeutic index.

Arry-520 has proved to be most effective in patients with relapsed or refractory multiple myeloma alone and in combination (17),(18), progressing to a phase III clinical trial and the possibility of becoming a valuable addition to the antimyeloma chemotherapeutic arsenal. Our studies here clearly show that Eg5 is the unique intracellular target for Arry-520 and thus offers an alternative way to target the cell cycle that differs from MT-targeting drugs currently used clinically to treat haematological cancers, such as vincristine.

Multiple myeloma is caused by clonal expansion of malignant plasma cells within the bone marrow (55). Acquired genetic mutations within myeloma cells and their interaction with bone marrow stromal cells contribute to disease progression and drug resistance. Evidence emerging from the sequencing of patients with multiple myeloma has revealed an extensive clonal heterogeneity even within the same individual (56). A recent phenotypic screening study using co-cultures of multiple myeloma cells with bone marrow stromal cells led to the identification and characterization of a novel ATP non-competitive Eg5 inhibitor BRD9647 that selectivity targeted myeloma cells over normal hematopoietic progenitors (13). Interestingly, a novel mutation in Eg5 at Y104C that is not located near the loop L5 allosteric binding site of other non-competitive inhibitors, caused resistance to BRD9647 suggesting it targets a distinct allosteric site. The current lack of clinical data associated with the long-term

use of Eg5 inhibitors in patients means information relating to acquired resistance will take time to emerge. It is therefore important to develop preclinical tools that can help predict the types and effects of mutations this class of compounds can generate during clinical evaluation and treatment, and understand the mechanisms at the molecular level that can lead to resistance. Our previous studies suggested that mutations in the L5 loop of Eg5 were scaffold independent (31), which had serious implications for drug design against this target. However, the sensitivity of the L214A mutant to ispinesib suggests that compounds can be engineered to avoid the reduced inhibition associated with some mutations that convey resistance across this class. Phenotypic screening employing the methods we describe here with a greater array of mutated cell lines, coupled with thermodynamic binding evaluations and structural and molecular dynamics studies should lead to a better understanding of the mechanisms that convey resistance at the target level, and enable the design of new inhibitors that can overcome these potentially clinically-relevant issues. Such inhibitors could then be used as suitable alternatives if acquired Eg5-related resistance to Arry-520 emerges during treatment, in a manner similar to the way that nilotinib succeeded imatinib when resistance was acquired during the treatment of patients with CML (57).

Keywords

Eg5, mitosis, Arry-520, resistance, multiple myeloma

Acknowledgements

This work used the platforms of the Grenoble Instruct-ERIC Center (ISBG: UMS 3518 CNRS-CEA-UGA-EMBL) with support from FRISBI (ANR-10-INSB-05-02) and GRAL (ANR-10-LABX-49-01) within the Grenoble Partnership for Structural Biology (PSB). We also thank Diamond Light Source for access to beamlines I04 and I04-1 (MX12305) that

contributed to the results presented here. Part of this work was supported by La Ligue Contre Le Cancer Comité du Rhône to DAS.

Authors' contributions

D.A.S and F.K. conceived the project and coordinated partner contributions. D.A.S and R.L.I. performed the cell biology, flow cytometry including microscopy and live cell imaging. S.K.T. grew crystals and solved the crystal structure. S.K.T. and F.K. performed structure refinement and analysis. F.L., S.H. and S.P.M. carried out the molecular dynamics simulations and analysis. D.A.S. wrote the manuscript with input from all authors.

References

1. Good JAD, Skoufias DA, Kozielski F. Elucidating the functionality of kinesins: an overview of small molecule inhibitors. Semin Cell Dev Biol. 2011;22:935–45.
2. Sawin KE, LeGuellec K, Philippe M, Mitchison TJ. Mitotic spindle organization by a plus-end-directed microtubule motor. Nature. 1992;359:540–3.
3. Scholey JE, Nithianantham S, Scholey JM, Al-Bassam J. Structural basis for the assembly of the mitotic motor Kinesin-5 into bipolar tetramers. eLife. 2014;3:e02217.
4. Blangy A, Arnaud L, Nigg EA. Phosphorylation by p34cdc2 protein kinase regulates binding of the kinesin-related motor HsEg5 to the dynactin subunit p150. J Biol Chem. 1997;272:19418–24.
5. Mayer TU, Kapoor TM, Haggarty SJ, King RW, Schreiber SL, Mitchison TJ. Small molecule inhibitor of mitotic spindle bipolarity identified in a phenotype-based screen. Science. 1999;286:971–4.
6. Rath O, Kozielski F. Kinesins and cancer. Nat Rev Cancer. 2012;12:527–39.
7. Yan Y, Sardana V, Xu B, Homnick C, Halczenko W, Buser CA, et al. Inhibition of a mitotic motor protein: where, how, and conformational consequences. J Mol Biol. 2004;335:547–54.
8. Maliga Z, Kapoor TM, Mitchison TJ. Evidence that monastrol is an allosteric inhibitor of the mitotic kinesin Eg5. Chem Biol. 2002;9:989–96.
9. Liu L, Parameswaran S, Liu J, Kim S, Wojcik EJ. Loop 5-directed compounds inhibit chimeric kinesin-5 motors: implications for conserved allosteric mechanisms. J Biol Chem. 2011;286:6201–10.
10. Kim ED, Buckley R, Learman S, Richard J, Parke C, Worthylake DK, et al. Allosteric drug discrimination is coupled to mechanochemical changes in the kinesin-5 motor core. J Biol Chem. 2010;285:18650–61.
11. Luo L, Parrish CA, Nevins N, McNulty DE, Chaudhari AM, Carson JD, et al. ATP-competitive inhibitors of the mitotic kinesin KSP that function via an allosteric mechanism. Nat Chem Biol. 2007;3:722–6.
12. Ulaganathan V, Talapatra SK, Rath O, Pannifer A, Hackney DD, Kozielski F. Structural insights into a unique inhibitor binding pocket in kinesin spindle protein. J Am Chem Soc. 2013;135:2263–72.
13. Chattopadhyay S, Stewart AL, Mukherjee S, Huang C, Hartwell KA, Miller PG, et al. Niche-Based Screening in Multiple Myeloma Identifies a Kinesin-5 Inhibitor with Improved Selectivity over Hematopoietic Progenitors. Cell Rep. 2015;10:755–70.
14. Yokoyama H, Sawada J, Katoh S, Matsuno K, Ogo N, Ishikawa Y, et al. Structural basis of new allosteric inhibition in Kinesin spindle protein Eg5. ACS Chem Biol. 2015;10:1128–36.
15. Shi J, Mitchison TJ. Cell death response to anti-mitotic drug treatment in cell culture, mouse tumor model and the clinic. Endocr Relat Cancer. 2017;24:T83–96.
16. Komlodi-Pasztor E, Sackett D, Wilkerson J, Fojo T. Mitosis is not a key target of microtubule agents in patient tumors. Nat Rev Clin Oncol. 2011;8:244–50.
17. Chari A, Htut M, Zonder JA, Fay JW, Jakubowiak AJ, Levy JB, et al. A phase 1 dose-escalation study of filanesib plus bortezomib and dexamethasone in patients with recurrent/refractory multiple myeloma. Cancer. 2016;122:3327–35.
18. Owens B. Kinesin inhibitor marches toward first-in-class pivotal trial. Nat Med.

2013;19:1550.
19. Shah JJ, Kaufman JL, Zonder JA, Cohen AD, Bensinger WI, Hilder BW, et al. A Phase 1 and 2 study of Filanesib alone and in combination with low-dose dexamethasone in relapsed/refractory multiple myeloma. Cancer. 2017;123:4617–30.
20. Tunquist BJ, Woessner RD, Walker DH. Mcl-1 stability determines mitotic cell fate of human multiple myeloma tumor cells treated with the kinesin spindle protein inhibitor ARRY-520. Mol Cancer Ther. 2010;9:2046–56.
21. Shi J, Orth JD, Mitchison T. Cell type variation in responses to antimitotic drugs that target microtubules and kinesin-5. Cancer Res. 2008;68:3269–76.
22. Tanenbaum ME, Macůrek L, Janssen A, Geers EF, Alvarez-Fernández M, Medema RH. Kif15 cooperates with eg5 to promote bipolar spindle assembly. Curr Biol CB. 2009;19:1703–11.
23. Sturgill EG, Norris SR, Guo Y, Ohi R. Kinesin-5 inhibitor resistance is driven by kinesin-12. J Cell Biol. 2016;213:213–27.
24. Tanenbaum ME, Macůrek L, Galjart N, Medema RH. Dynein, Lis1 and CLIP-170 counteract Eg5-dependent centrosome separation during bipolar spindle assembly. EMBO J. 2008;27:3235–45.
25. Maliga Z, Mitchison TJ. Small-molecule and mutational analysis of allosteric Eg5 inhibition by monastrol. BMC Chem Biol. 2006;6:2.
26. Brier S, Lemaire D, DeBonis S, Forest E, Kozielski F. Molecular dissection of the inhibitor binding pocket of mitotic kinesin Eg5 reveals mutants that confer resistance to antimitotic agents. J Mol Biol. 2006;360:360–76.
27. Wacker SA, Houghtaling BR, Elemento O, Kapoor TM. Using transcriptome sequencing to identify mechanisms of drug action and resistance. Nat Chem Biol. 2012;8:235–7.
28. Indorato R-L, DeBonis S, Kozielski F, Garcia-Saez I, Skoufias DA. STLC-resistant cell lines as tools to classify chemically divergent Eg5 targeting agents according to their mode of action and target specificity. Biochem Pharmacol. 2013;86:1441–51.
29. Tcherniuk S, van Lis R, Kozielski F, Skoufias DA. Mutations in the human kinesin Eg5 that confer resistance to monastrol and S-trityl-L-cysteine in tumor derived cell lines. Biochem Pharmacol. 2010;79:864–72.
30. Skoufias DA, DeBonis S, Saoudi Y, Lebeau L, Crevel I, Cross R, et al. S-trityl-L-cysteine is a reversible, tight binding inhibitor of the human kinesin Eg5 that specifically blocks mitotic progression. J Biol Chem. 2006;281:17559–69.
31. Talapatra SK, Anthony NG, Mackay SP, Kozielski F. Mitotic kinesin Eg5 overcomes inhibition to the phase I/II clinical candidate SB743921 by an allosteric resistance mechanism. J Med Chem. 2013;56:6317–29.
32. Souid A-K, Dubowy RL, Ingle AM, Conlan MG, Sun J, Blaney SM, et al. A pediatric phase I trial and pharmacokinetic study of ispinesib: a Children's Oncology Group phase I consortium study. Pediatr Blood Cancer. 2010;55:1323–8.
33. Talapatra SK, Schüttelkopf AW, Kozielski F. The structure of the ternary Eg5-ADP-ispinesib complex. Acta Crystallogr D Biol Crystallogr. 2012;68:1311–9.
34. Kaan HYK, Ulaganathan V, Hackney DD, Kozielski F. An allosteric transition trapped in an intermediate state of a new kinesin-inhibitor complex. Biochem J. 2009;425:55–60.
35. Battye TGG, Kontogiannis L, Johnson O, Powell HR, Leslie AGW. iMOSFLM: a new graphical interface for diffraction-image processing with MOSFLM. Acta Crystallogr D Biol Crystallogr. 2011;67:271–81.
36. Winn MD, Ballard CC, Cowtan KD, Dodson EJ, Emsley P, Evans PR, et al. Overview of the CCP4 suite and current developments. Acta Crystallogr D Biol Crystallogr.

2011;67:235–42.
37. Maliga Z, Xing J, Cheung H, Juszczak LJ, Friedman JM, Rosenfeld SS. A pathway of structural changes produced by monastrol binding to Eg5. J Biol Chem. 2006;281:7977–82.
38. Murshudov GN, Vagin AA, Dodson EJ. Refinement of macromolecular structures by the maximum-likelihood method. Acta Crystallogr D Biol Crystallogr. 1997;53:240–55.
39. Adams PD, Afonine PV, Bunkóczi G, Chen VB, Davis IW, Echols N, et al. PHENIX: a comprehensive Python-based system for macromolecular structure solution. Acta Crystallogr D Biol Crystallogr. 2010;66:213–21.
40. Case DA, Cheatham TE, Darden T, Gohlke H, Luo R, Merz KM, et al. The Amber biomolecular simulation programs. J Comput Chem. 2005;26:1668–88.
41. Singh UC, Kollman PA. An Approach to Computing Electrostatic Charges for Molecules. J Comput Chem. 1984;5, 129–45.
42. Meagher KL, Redman LT, Carlson HA. Development of polyphosphate parameters for use with the AMBER force field. J Comput Chem. 2003;24:1016–25.
43. Hornak V, Abel R, Okur A, Strockbine B, Roitberg A, Simmerling C. Comparison of multiple Amber force fields and development of improved protein backbone parameters. Proteins. 2006;65:712–25.
44. Mark P, Nillson L. Structure and Dynamics of the TIP3P, SPC, and SPC/E Water Models at 298 K. J Phys Chem A. 2001;9954–9960.
45. Harvey MJ, Giupponi G, Fabritiis GD. ACEMD: Accelerating Biomolecular Dynamics in the Microsecond Time Scale. J Chem Theory Comput. 2009;5:1632–9.
46. Feenstra KA, Hess B, Berendsen HJ. Improving efficiency of large time-scale molecular dynamics simulations of hydrogen-rich systems. J Comput Chem. 20th ed. 1999;786–98.
47. Humphrey W, Dalke A, Schulten K. VMD: visual molecular dynamics. J Mol Graph. 1996;14:33–8, 27–8.
48. Lemeiux C, DeWolf W, Voegtli W, et al. ARRY-520, a novel, highly selective KSP inhibitor with potent anti-proliferative activity. Proc Am Assoc Cancer Res. 2007;48: 5590.
49. Turner J, Anderson R, Guo J, Beraud C, Fletterick R, Sakowicz R. Crystal structure of the mitotic spindle kinesin Eg5 reveals a novel conformation of the neck-linker. J Biol Chem. 2001;276:25496–502.
50. Kaan HYK, Major J, Tkocz K, Kozielski F, Rosenfeld SS. "Snapshots" of ispinesib-induced conformational changes in the mitotic kinesin Eg5. J Biol Chem. 2013;288:18588–98.
51. Lad L, Luo L, Carson JD, Wood KW, Hartman JJ, Copeland RA, et al. Mechanism of inhibition of human KSP by ispinesib. Biochemistry. 2008;47:3576–85.
52. Talapatra SK, Tham CL, Guglielmi P, Cirilli R, Chandrasekaran B, Karpoormath R, et al. Crystal structure of the Eg5 - K858 complex and implications for structure-based design of thiadiazole-containing inhibitors. Eur J Med Chem. 2018;156:641–51.
53. Khoury HJ, Garcia-Manero G, Borthakur G, Kadia T, Foudray MC, Arellano M, et al. A phase 1 dose-escalation study of ARRY-520, a kinesin spindle protein inhibitor, in patients with advanced myeloid leukemias. Cancer. 2012;118:3556–64.
54. Drewinko B, Alexanian R, Boyer H, Barlogie B, Rubinow SI. The growth fraction of human myeloma cells. Blood. 1981;57:333–8.
55. Hideshima T, Mitsiades C, Tonon G, Richardson PG, Anderson KC. Understanding multiple myeloma pathogenesis in the bone marrow to identify new therapeutic targets. Nat Rev Cancer. 2007;7:585–98.
56. Lohr JG, Stojanov P, Carter SL, Cruz-Gordillo P, Lawrence MS, Auclair D, et al. Widespread genetic heterogeneity in multiple myeloma: implications for targeted therapy. Cancer Cell. 2014;25:91–101.

57. Giles FJ, le Coutre PD, Pinilla-Ibarz J, Larson RA, Gattermann N, Ottmann OG, et al. Nilotinib in imatinib-resistant or imatinib-intolerant patients with chronic myeloid leukemia in chronic phase: 48-month follow-up results of a phase II study. Leukemia. 2013;27:107–12.
58. Laskowski RA, Swindells MB. LigPlot+: multiple ligand-protein interaction diagrams for drug discovery. J Chem Inf Model. 2011;51:2778–86.

Table 1 Mitotic fate of individual naïve U2OS and Eg5(D130A) or Eg5(L214A) expressing U2OS cells in the presence of allosteric Eg5 inhibitors followed by time-lapse video.

U2OS cells, treatment	**# M cells observed**	**# M normal (% total)**	**# M arrested (% total)**	**# M exit aberrant (% total)**
Naïve untreated	192	94.8	0.5	4.7
Naïve + Arry-520	297	1.3	85.2	13.5
Eg5(D130A) + STLC	176	89.8	1.1	9.1
Eg5(D130A) + Arry-520	642	51.4	38.3	10.3
Eg5(D130A) + ispinesib	140	87.1	2.9	10.0
Eg5(L214A) + STLC	290	94.5	0.3	5.2
Eg5(L214A) + Arry-520	680	91.8	3.8	4.4
Eg5(L214A) + ispinesib	130	2.3	84.6	13.1

Table 2 Time which naïve, Eg5(D130A) or Eg5(L214A) expressing U2OS cells spent in mitosis, in the presence of allosteric Eg5 inhibitors, leading to successful cytokinesis.

U2OS cells, treatment	**# cells that spent ≤ 60 min in M (% of total M cells)**	**# cells that spent ≤ 120 min in M (% of total M cells)**
Naïve untreated	90.1	97.2
Eg5(D130A) + STLC	89.2	100
Eg5(D130A) + Arry-520	51.8	67.7
Eg5(D130A) + ispinesib	79.5	95.1
Eg5(L214A) + STLC	90.2	99.3
Eg5(L214A) + Arry-520	84.7	94.9

Figure legends

Figure 1. *Structure of the Eg5-Arry-520 complex*. a) Chemical structure of Arry-520. b) Raw data (top) and integrated data (bottom) from ITC measurements demonstrating high picomolar affinity and exothermic reaction upon sequential additions of Arry-520 to Eg5. c) Overall structure of the ternary Mg^{2+}ADP–Eg5–Arry-520 complex showing the front view of the Eg5 motor domain with bound Mg^{2+} (red), ADP (green/orange) and Arry-520 (magenta). d) Magnification of the allosteric binding pocket of Eg5 (yellow) composed of helix α2, loop L5 and helix α3 with Arry-520 (magenta) and the electron density omit map (colored in blue) contoured at 3σ. e) Stereo plot of Arry-520 (magenta) and surrounding residues of the inhibitor binding pocket (colored in cyan). f) Comparison of the distinct binding modes of Arry-520 (magenta) and ispinesib (green); the protein surface is displayed semi-transparently.

Figure 2. *Cell cycle progression and spindle formation in naïve* U2OS cells and cells expressing *either Eg5(D130A) or Eg5(L214A) STLC resistant clones in the presence of Arry-520 or ispinesib*. a) Cell cycle distribution of cells after 24 h treatment with either 10 μM STLC, 10 nM Arry-520 or 10 nM ispinesib. Naive U2OS cell were blocked in 4N in the presence of either STLC, Arry-520 or ispinesib whereas U2OS cells expressing either Eg5(D130A) or Eg5(L214) were resistant to STLC and Arry-520 having normal cell cycle profiles as the untreated control cells. In stark contrast, U2OS cells expressing Eg5(L214A) cells were sensitive to ispinesib and they accumulated at 4N. b) Immunofluorescence microscopy of cells stained with anti-β-tubulin for microtubule staining showing induction of monoastral spindles following treatment with Arry-520 in U2OS cells. U2OS cells previously selected to be resistant to STLC due to expression of either Eg5(D130A) or Eg5(L214A) were also capable of forming normal bipolar spindles in the presence of Arry-520. In stark contrast

to Eg5(D130A) expressing U2OS cells, the Eg5(L214A) expressing cells were still sensitive to ispinesib as shown by the presence of monoastral spindles. Scale bar = 10 μm. c) Cells were treated with either 10 μM STLC (solid black bars), 10 nM Arry-520 (dark gray bars) or 10 nM ispinesib (light gray bars) for 8 h and then were fixed and stained for immunofluorescence microscopy as in panel b. The percentage of monoastral spindles from the total number of mitotic cells was then quantified.

Figure 3. *Duration of mitosis and colony formation of U2OS cells expressing either Eg5(D130A) or Eg5(L214A) STLC resistant clones in the continuous presence of STLC, Arry-520 or ispinesib*. After addition of 10 μM STLC, 10 nM Arry-520 or 10 nM ispinesib cells were recorded for 16 h by time-lapse video microscopy and the time that each cell spent in mitosis was scored. The time of each cell that successfully completed mitosis is plotted against the number of cells (number in parenthesis at each condition). b) Cells (2k) following seeding were treated with either 10 μM STLC, 10 nM Arry-520 or 10 nM ispinesib and allowed to proliferate for 10 days. Cells were then fixed and stained with crystal violet. c) U2OS cell expressing either Eg5(D130A) or Eg5(L214A) were plated at a density of 17,000 cells per well in 24-well plates in the absence or in the presence of 10 □M STLC 10 nM Arry-520, or 10 nM Ispinesib. Following treatment for four days, cells were fixed with 4% paraformaldehyde and stained with 0.5% Crystal Violet. Shown are representative images of two wells from experiments performed in triplicate. d) Quantitation of c) as per absorbance at 595 nm normalized relative to the untreated cells. $*p < 0.05$.

Figure 4. *Flexibility of Arry-520 and ispinesib in the allosteric binding site*. Arry-520 binding in WT Eg5 (a), D130A (b) and L214A(c) Eg5 mutants. Ispinesib (ISP) binding in WT (a'), D130A (b') and L214A (c') mutants. The spatial position of wild type residues (labeled in

black) and mutations (labeled in red) is illustrated as sticks. Structural flexibility (shown in cyan) of ispinesib is similar in both wild type Eg5 and the Eg5(L214A) mutant, but higher in D130A. Arry-520 is less flexible in the wild type and more so in the Eg5(L214A) and Eg5(D130A) mutants. The structural dynamics of Arry-520 and ispinesib over the course the simulations are illustrated as cyan lines. The final conformations of the drugs are illustrated as cyan sticks. Rotations of the indicated bonds (indicated by red asterisks) take place around the bond between d) the 2,5-difluorophenyl group and the 1,3,4-thiadiazole ring in Arry-520 and e) the quinazolin-4-one ring and the isopropyl group in ispinesib. f) Bond angle flexibility in wild type Eg5 is shown in black, in blue for the Eg5(D130A) mutant and in red color for the Eg5(L214A) mutant.

Figure 1

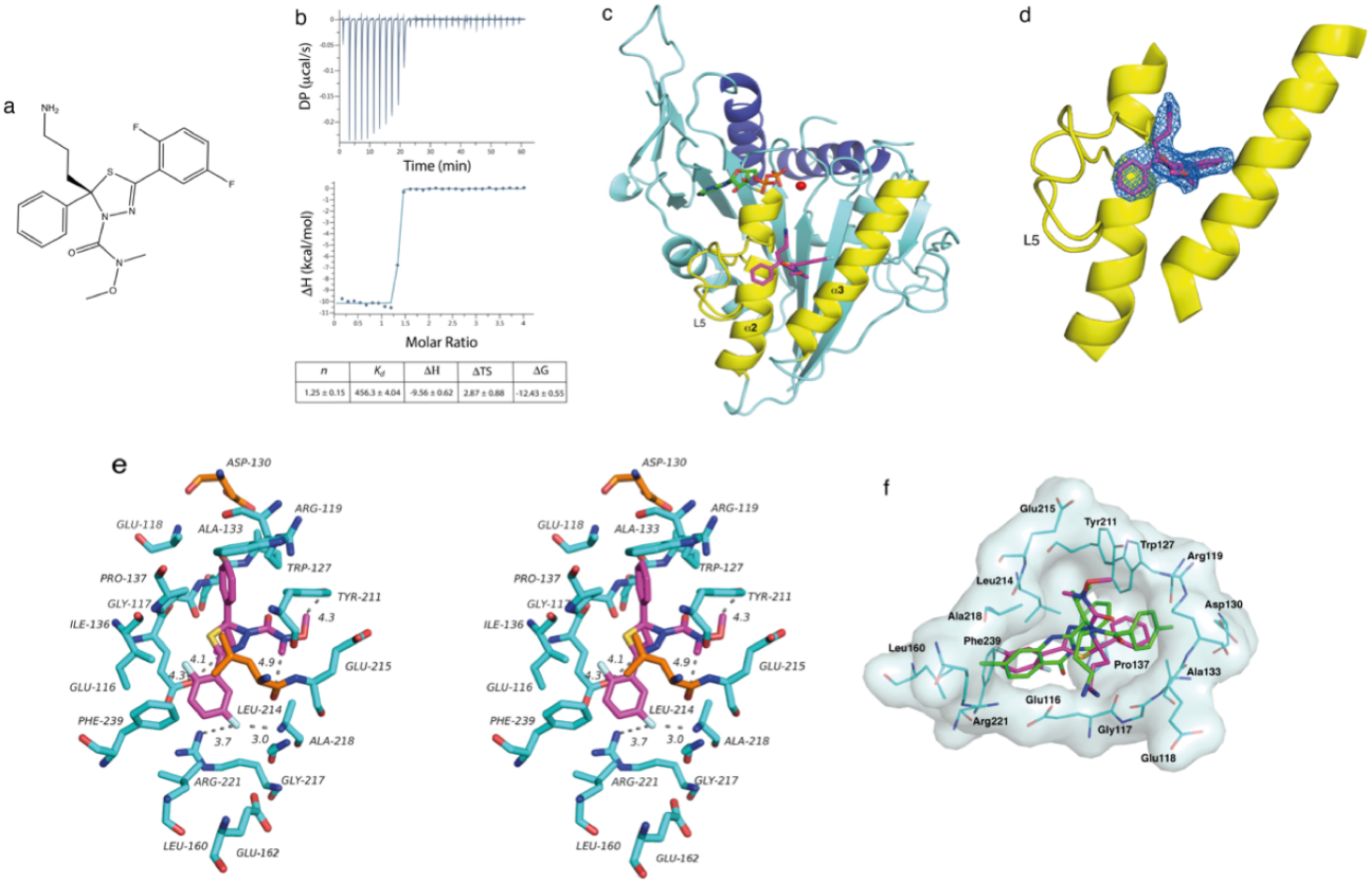

n	K_d	ΔH	ΔTS	ΔG
1.25 ± 0.15	456.3 ± 4.04	-9.56 ± 0.62	2.87 ± 0.88	-12.43 ± 0.55

Figure 2

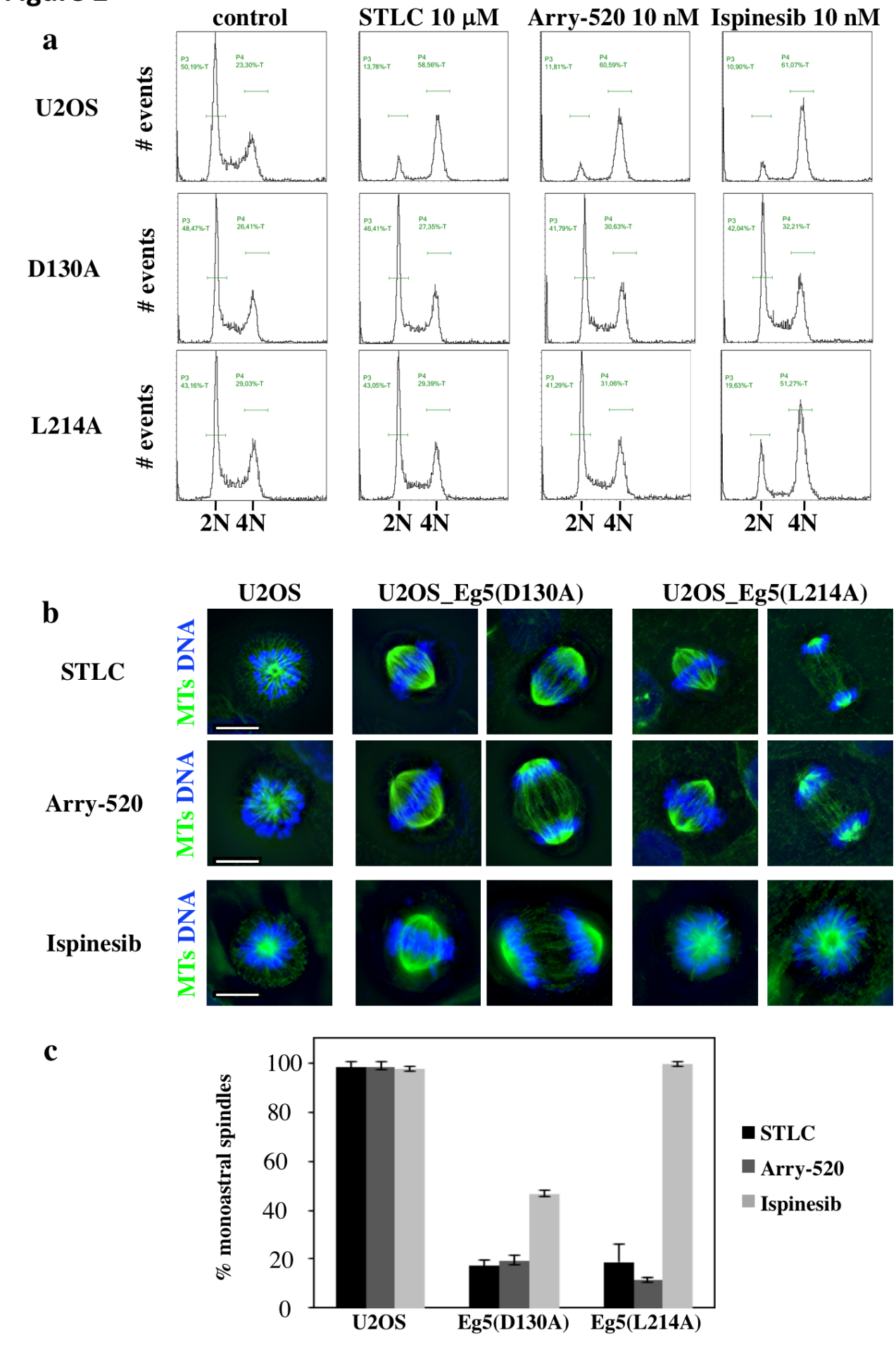
a
control
STLC 10 µM
Arry-520 10 nM
Ispinesib 10 nM
U2OS
D130A
L214A
events
2N 4N
b
U2OS
U2OS_Eg5(D130A)
U2OS_Eg5(L214A)
STLC
Arry-520
Ispinesib
MTs DNA
c
% monoastral spindles
100
80
60
40
20
0
U2OS
Eg5(D130A)
Eg5(L214A)
STLC
Arry-520
Ispinesib

Figure 3

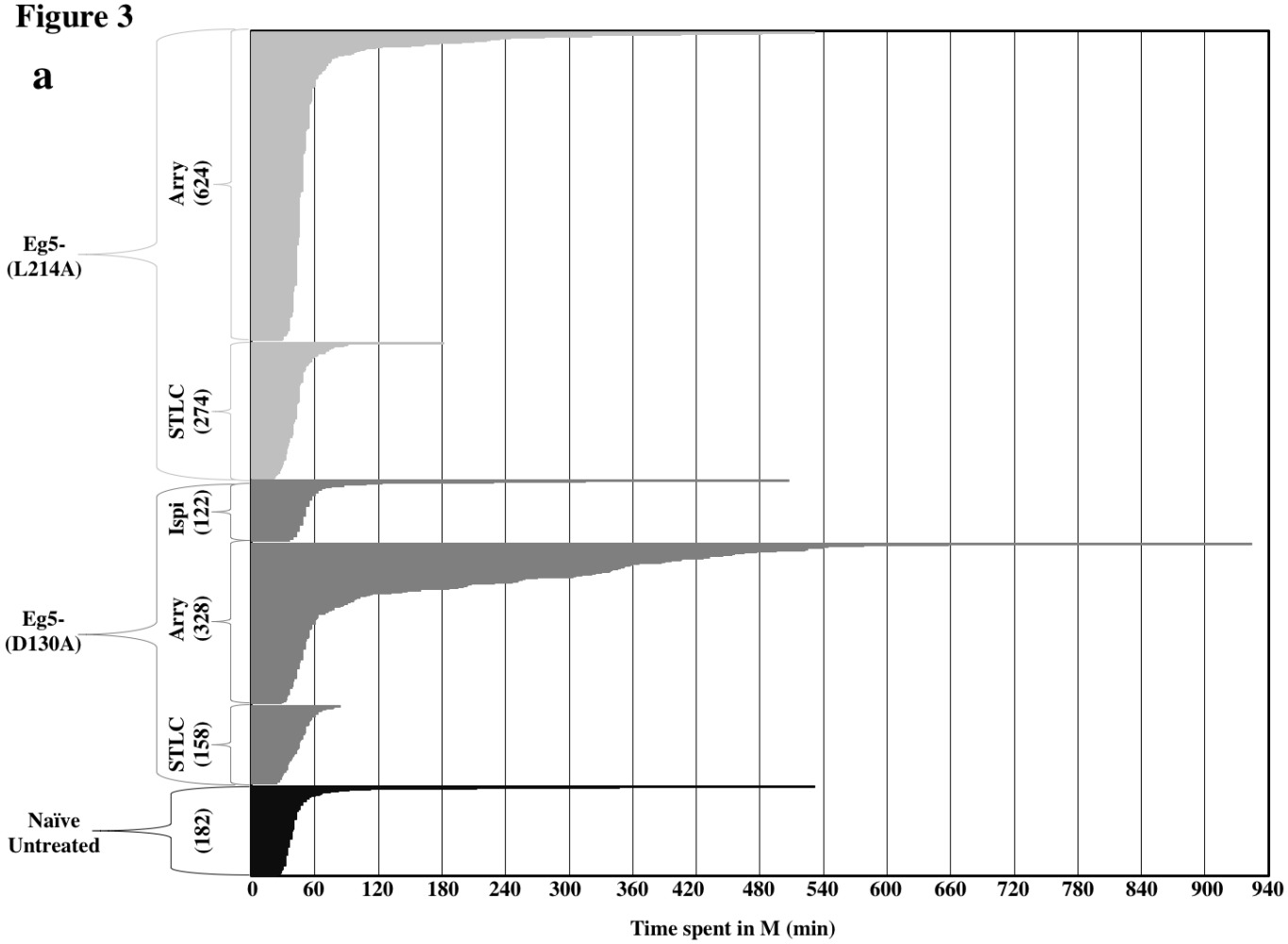
a
Eg5-
(L214A)
Arry
(624)
STLC
(274)
Ispi
(122)
Eg5-
(D130A)
Arry
(328)
STLC
(158)
Naïve
Untreated
(182)
0
60
120
180
240
300
360
420
480
540
600
660
720
780
840
900
940
Time spent in M (min)

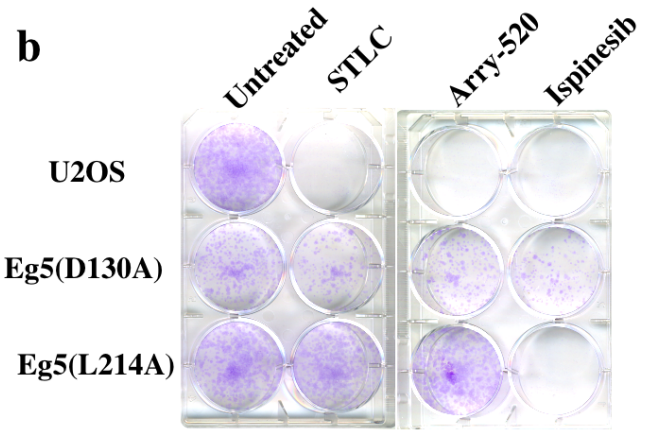
b
Untreated
STLC
Arry-520
Ispinesib
U2OS
Eg5(D130A)
Eg5(L214A)

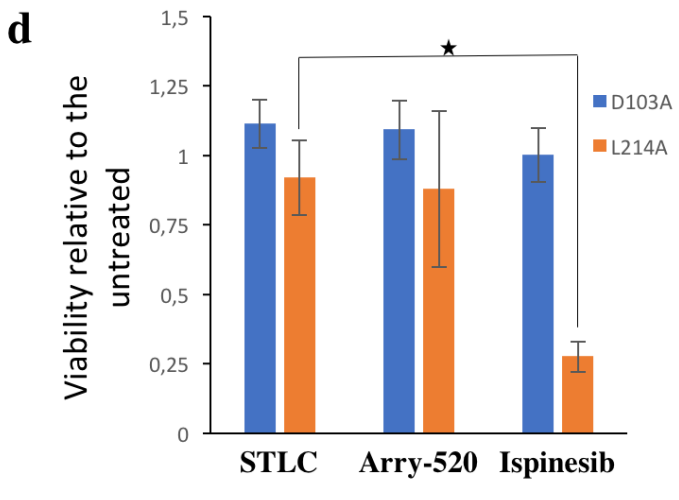
d
Viability relative to the untreated
1,5
1,25
1
0,75
0,5
0,25
0
D103A
L214A
STLC
Arry-520
Ispinesib

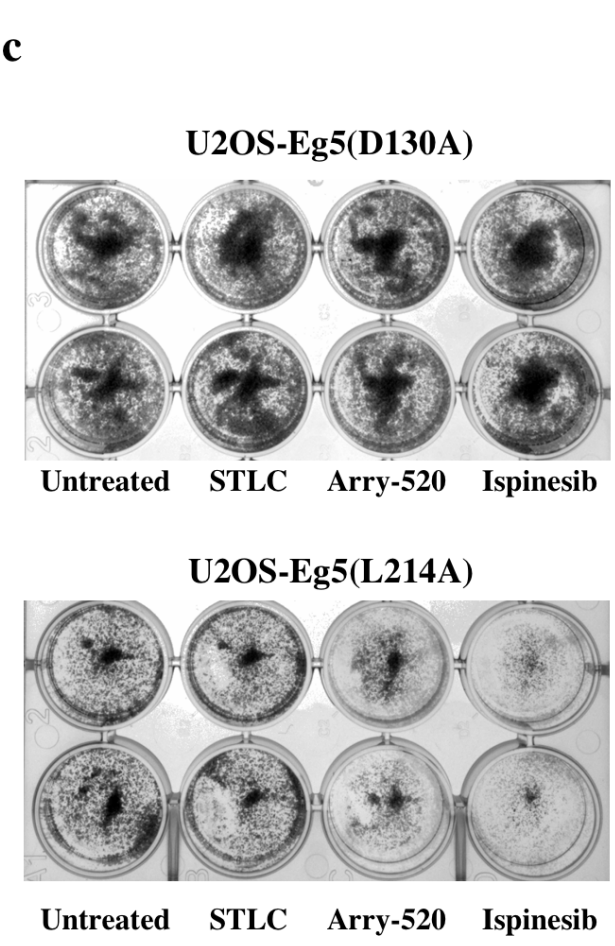
c
U2OS-Eg5(D130A)
Untreated
STLC
Arry-520
Ispinesib
U2OS-Eg5(L214A)
Untreated
STLC
Arry-520
Ispinesib

Figure 4

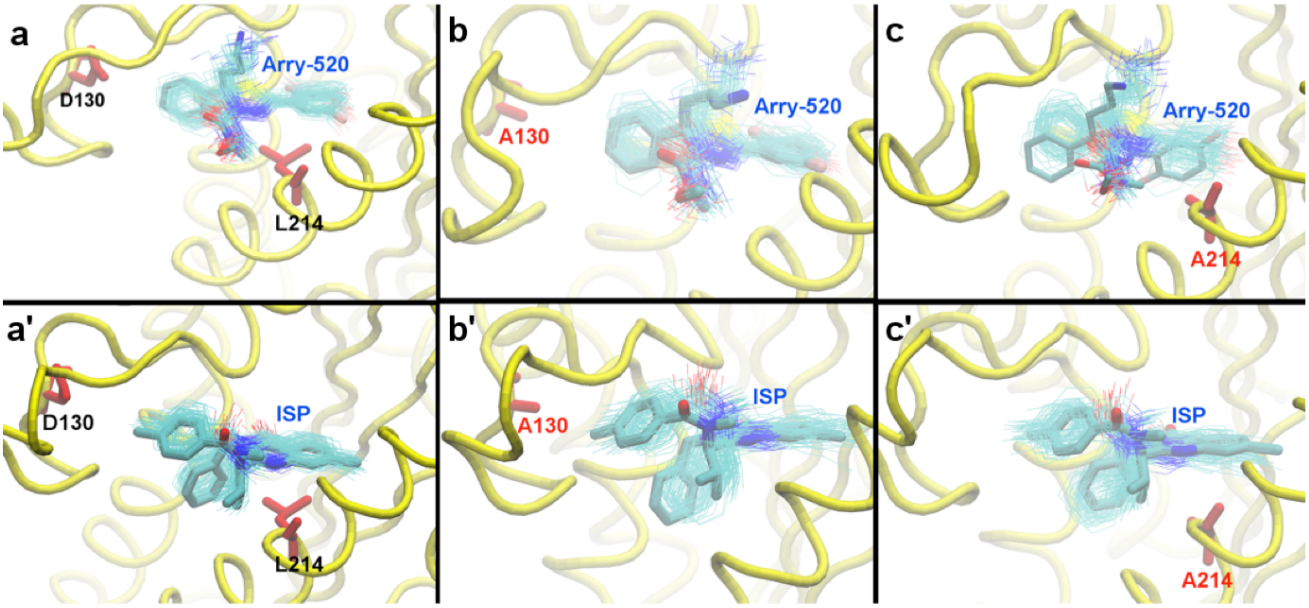
a
Arry-520
D130
L214
b
Arry-520
A130
c
Arry-520
A214
a'
ISP
D130
L214
b'
ISP
A130
c'
ISP
A214

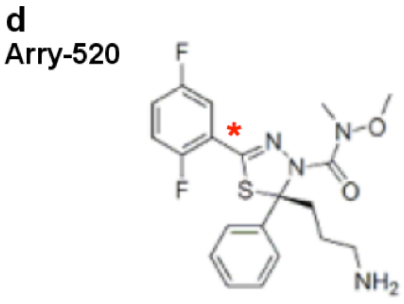
d
Arry-520
F
F
*
N
N
S
N-O
O
NH2

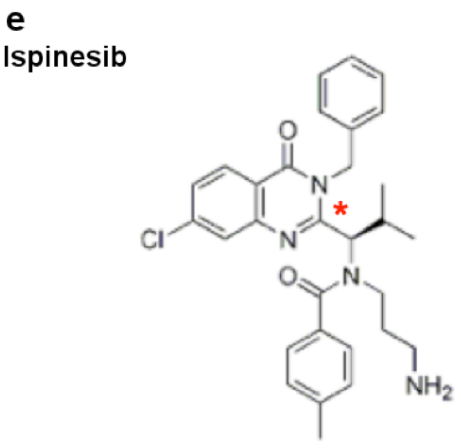
e
Ispinesib
Cl
O
N
*
N
O
N
NH2

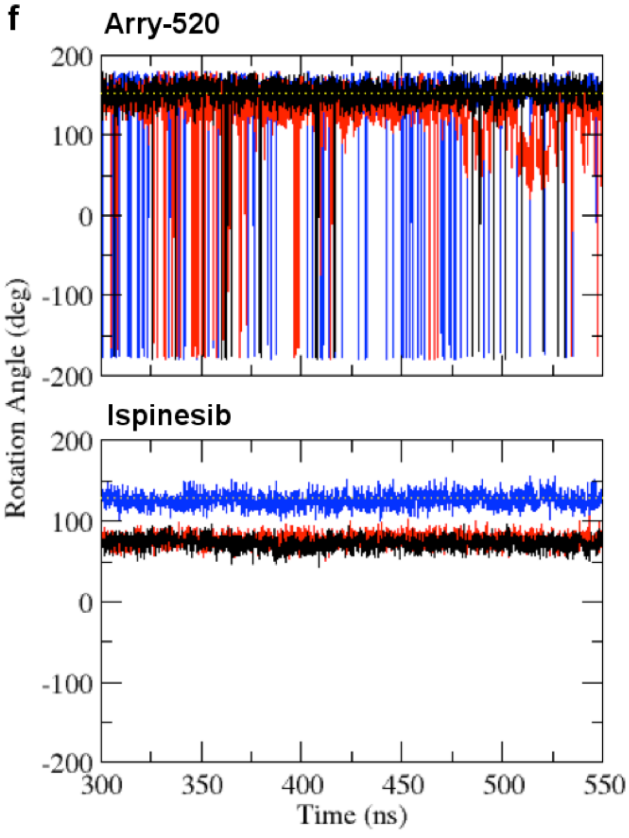
f
Arry-520
Ispinesib
Rotation Angle (deg)
200
100
0
-100
-200
300
350
400
450
500
550
Time (ns)